

IFT88 controls NuMA enrichment at k-fibers minus-ends to facilitate their re-anchoring into mitotic spindles

Nicolas Taulet, Audrey Douanier, Benjamin Vitre, Christelle Anguille, Justine Maurin, Yann Dromard, Virginie Georget, Benedicte Delaval

▶ **To cite this version:**

Nicolas Taulet, Audrey Douanier, Benjamin Vitre, Christelle Anguille, Justine Maurin, et al.. IFT88 controls NuMA enrichment at k-fibers minus-ends to facilitate their re-anchoring into mitotic spindles. Scientific Reports, 2019, 9 (1), pp.10311. 10.1038/s41598-019-46605-x . hal-02339016

HAL Id: hal-02339016
https://hal.umontpellier.fr/hal-02339016

Submitted on 25 May 2021

HAL is a multi-disciplinary open access archive for the deposit and dissemination of scientific research documents, whether they are published or not. The documents may come from teaching and research institutions in France or abroad, or from public or private research centers.

L'archive ouverte pluridisciplinaire **HAL**, est destinée au dépôt et à la diffusion de documents scientifiques de niveau recherche, publiés ou non, émanant des établissements d'enseignement et de recherche français ou étrangers, des laboratoires publics ou privés.



Distributed under a Creative Commons Attribution 4.0 International License

SCIENTIFIC REPORTS

OPEN

IFT88 controls NuMA enrichment at k-fibers minus-ends to facilitate their re-anchoring into mitotic spindles

Received: 27 December 2018
Accepted: 2 July 2019
Published online: 16 July 2019

Nicolas Taulet[1], Audrey Douanier[1], Benjamin Vitre[1], Christelle Anguille[1], Justine Maurin[1], Yann Dromard[2], Virginie Georget[2] & Benedicte Delaval[1]

To build and maintain mitotic spindle architecture, molecular motors exert spatially regulated forces on microtubules (MT) minus-ends. This spatial regulation is required to allow proper chromosomes alignment through the organization of kinetochore fibers (k-fibers). NuMA was recently shown to target dynactin to MT minus-ends and thus to spatially regulate dynein activity. However, given that k-fibers are embedded in the spindle, our understanding of the machinery involved in the targeting of proteins to their minus-ends remains limited. Intraflagellar transport (IFT) proteins were primarily studied for their ciliary roles but they also emerged as key regulators of cell division. Taking advantage of MT laser ablation, we show here that IFT88 concentrates at k-fibers minus-ends and is required for their re-anchoring into spindles by controlling NuMA accumulation. Indeed, IFT88 interacts with NuMA and is required for its enrichment at newly generated k-fibers minus-ends. Combining nocodazole washout experiments and IFT88 depletion, we further show that IFT88 is required for the reorganization of k-fibers into spindles and thus for efficient chromosomes alignment in mitosis. Overall, we propose that IFT88 could serve as a mitotic MT minus-end adaptor to concentrate NuMA at minus-ends thus facilitating k-fibers incorporation into the main spindle.

The mitotic spindle is a highly dynamic structure that is essential for mammalian cell division[1]. Indeed, proper bipolar mitotic spindle architecture is essential for both spindle orientation and for proper chromosomes alignment in metaphase. To assemble itself and preserve its integrity, the mitotic spindle must continuously coordinate microtubule (MT) nucleation with the integration of various MT structures[1–3]. Indeed, at mitotic entry, peripheral acentrosomal MTs form clusters that move and integrate into the forming spindle[4,5]. Similarly, kinetochore nucleated k-fibers continuously need to be integrated into the main spindle by sliding towards the poles to ensure efficient spindle assembly and proper chromosomes alignment[6–8]. Such a coordination is achieved by the action of MT associated proteins (MAPs) and motors that exert spatially regulated forces on MTs to cluster them into poles. MT minus-ends, which are clustered at the spindle poles, can be considered as a platform for such a regulation. Indeed, the Nuclear Mitotic Apparatus protein (NuMA) was recently shown to target dynactin to minus-ends and thus spatially regulate dynein activity[8,9]. If proteins recruitment at MT plus-end has been well-documented, the specific targeting of proteins to MTs and k-fiber minus-ends has yet to be fully understood[10]. Indeed, continuous reintegration of k-fibers happens inside an established spindle and is essential to preserve its integrity and to ensure proper chromosomes alignment[6–8]. However, given that k-fibers are embedded into the main spindle, our understanding of the machinery involved in the targeting of proteins to their minus-ends remains limited.

The IntraFlagellar Transport (IFT) machinery is a well conserved intracellular transport system that has been studied for a long time for its role in cilia formation and function in non-dividing cells[11]. During IFT-mediated transport, kinesin and dynein motors drive the bidirectional transport of IFT trains from the base to the tip of the cilium in an anterograde movement and from the tip to the base in a retrograde movement[12]. IFTs were therefore accepted to function as cargos, for example, of axoneme precursors such as tubulins as well as molecules of the

[1]CRBM, CNRS, Univ. Montpellier, Centrosome, cilia and pathologies Lab, 1919 Route de Mende, 34293, Montpellier, France. [2]Montpellier Ressources Imagerie, CRBM, CNRS, Univ. Montpellier, 1919 Route de Mende, 34293, Montpellier, France. Nicolas Taulet and Audrey Douanier contributed equally. Correspondence and requests for materials should be addressed to N.T. (email: nicolastaulet@hotmail.com) or B.D. (email: benedicte.delaval@crbm.cnrs.fr)

signal transduction machinery inside the cilium[13,14]. More recently, IFTs were shown to contribute to ciliary motor activation[15] indicating that a lot remains to be done to fully understand the roles of this complex machinery. Interestingly, in addition to their ciliary roles, IFTs were also shown to function in interphase in the regulation of MT dynamics in the cytoplasm[16]. Moreover, they were shown to contribute to intracellular transport in non-ciliary systems such as lymphocytes[17,18] or dividing cells[19,20]. Indeed, in mitosis, IFT88 was previously shown to function as part of a dynein1-driven complex required for the transport of peripheral MT clusters to spindle poles to ensure proper formation of astral MT arrays and correct spindle orientation[19]. Recent results also indicate that IFT88 is required for central spindle organization[20]. However, the requirement of IFT proteins for k-fibers organization has never been directly addressed.

Here, taking advantage of MT laser ablation, we show that IFT88, a core member of the IFT machinery, concentrates at k-fibers minus-ends and is required for their re-anchoring into spindles by controlling NuMA accumulation. Mechanistically, IFT88 interacts with NuMA and is required for its enrichment at newly generated k-fibers minus-ends. Combining nocodazole washout experiments and IFT88 depletion, we further confirm that IFT88 is required for the reorganization of k-fibers into spindles and subsequent efficient chromosomes alignment in mitosis. These findings identify a new mechanism for NuMA enrichment at k-fibers minus-ends involving a core member of the IFT machinery. Indeed, we propose that IFT88 could serve as a mitotic minus-ends adaptor to concentrate NuMA at k-fiber minus-ends thus facilitating their incorporation into the main spindle and subsequent chromosomes alignment.

Results

IFT88 concentrates at the newly generated k-fiber minus-end after laser ablation. The spindle must continuously coordinate MTs nucleation with the integration of kinetochores bound k-fibers in order to properly control chromosomes alignment. Poleward movement of k-fibers thus continuously happens inside an established spindle[8] but is difficult to observe due to the dense array of MTs in this region. Indeed, k-fibers are embedded in the spindle and their minus-ends are not easy to image. To overcome this challenge and test whether IFT88 could be required for k-fibers re-incorporation into spindles, we took advantage of MT laser ablation to create new and isolated k-fibers minus-ends in an established spindle. This technique allows to visualize in bipolar or monopolar spindles the reintegration and subsequent transport of both MTs and k-fibers into the spindle[8]. To dynamically visualize protein recruitment at newly generated k-fibers minus-ends after laser ablation and determine if IFT88 could be recruited at this site, we performed time-lapse imaging on an Emerald-IFT88 cell line. Upon laser ablation, Emerald-IFT88 was found to rapidly accumulate at the newly generated MT minus-end (Fig. 1a,b; Supplementary Movie 1). This accumulation of IFT88 at the newly generated minus-end was consistent with the idea that IFT88 could be required for k-fibers re-incorporation into spindles.

IFT88 contributes to k-fibers re-anchoring into spindles after laser ablation. To test whether IFT88 could participate in k-fibers re-incorporation into spindles, we performed time-lapse imaging on GFP-α-tubulin cells[5] and monitored k-fibers re-anchoring after ablation upon control and IFT88-depleted conditions (Fig. 1c–e; Supplementary Fig. 1a–c; Movie 2). IFT88 depletion using two independent siRNA (IFT88 and IFT88 #2) was controlled by western-blot (Fig. 1c; Supplementary Figs 1a and 3a,b) and Hoechst live staining was combined to GFP-α-tubulin to allow chromosomes visualization. In control condition, as previously shown[8], detached k-fibers rapidly re-anchored to the neighboring MTs and were transported back towards the pole (Fig. 1d,e; Supplementary Fig. 1b,c). In contrast, k-fibers re-anchoring was significantly delayed upon IFT88 depletion (Fig. 1d,e; Supplementary Fig. 1b,c). These results indicate that, upon laser ablation, IFT88, which accumulates at the newly generated minus-end, is required for efficient k-fibers re-anchoring into spindles.

IFT88 interacts with NuMA and is required for its minus-end enrichment. K-fibers re-incorporation was previously shown to depend on NuMA accumulation at the newly generated minus-end[8]. Subsequently, dynein activity is recruited at this location to allow proper re-anchoring of ablated MTs to the spindle[9]. However, how NuMA accumulates at k-fiber minus-ends is not completely understood. The rapid enrichment in IFT88 observed at minus-end after ablation (Fig. 1a,b) suggested that IFT88 could be required for NuMA accumulation at this site. To test this hypothesis, we generated new and resolvable k-fibers minus-ends using laser ablation on monopolar spindles and monitored NuMA enrichment upon control and IFT88-depleted conditions (Fig. 2a–c; Supplementary Movie 3). More specifically, a YFP-NuMA cell line was used to dynamically monitor by live imaging the impact of IFT88 depletion on the recruitment of NuMA at the newly generated k-fiber minus-end after ablation. As previously described, NuMA rapidly localized at new minus-end structures and accumulated there before their re-incorporation into the main spindle (Fig. 2a–c). However, the striking accumulation of NuMA observed at the ablated k-fibers minus-ends in control cells was decreased in IFT88-depleted cells (Fig. 2a–c). Indeed, only 24% of newly generated minus-ends presented with NuMA accumulation compared to 68% in control condition (Fig. 2b). The decrease in NuMA intensity was further validated by fluorescence intensity quantifications (Fig. 2c). Of note, a weak NuMA signal remained after IFT88 depletion due either to a residual expression of IFT88 or to NuMA binding to MTs independently of IFT88. Also in agreement with a role for IFT88 in allowing NuMA accumulation at MTs minus-end after ablation, fluorescence intensity measurements of IFT88 and NuMA accumulation over time at the newly generated minus-end showed that IFT88 accumulated before NuMA (Fig. 2d; Supplementary Fig. 2). IFT88 accumulation then decreased as k-fibers re-anchored into the main spindle (Fig. 2d; Supplementary Fig. 2). To further confirm that IFT88 and NuMA could function together, we assessed whether they could interact in mitosis, performing co-immunoprecipitation (Fig. 2e; Supplementary Fig. 3c). LLC-PK1 cells were synchronized in mitosis using nocodazole and enriched in acentrosomal MT asters using nocodazole washout for 3 min. Endogenous immunoprecipitation of IFT88 revealed a co-immunoprecipitation with NuMA in mitotic cells. Collectively, these results showed that IFT88 interacts with

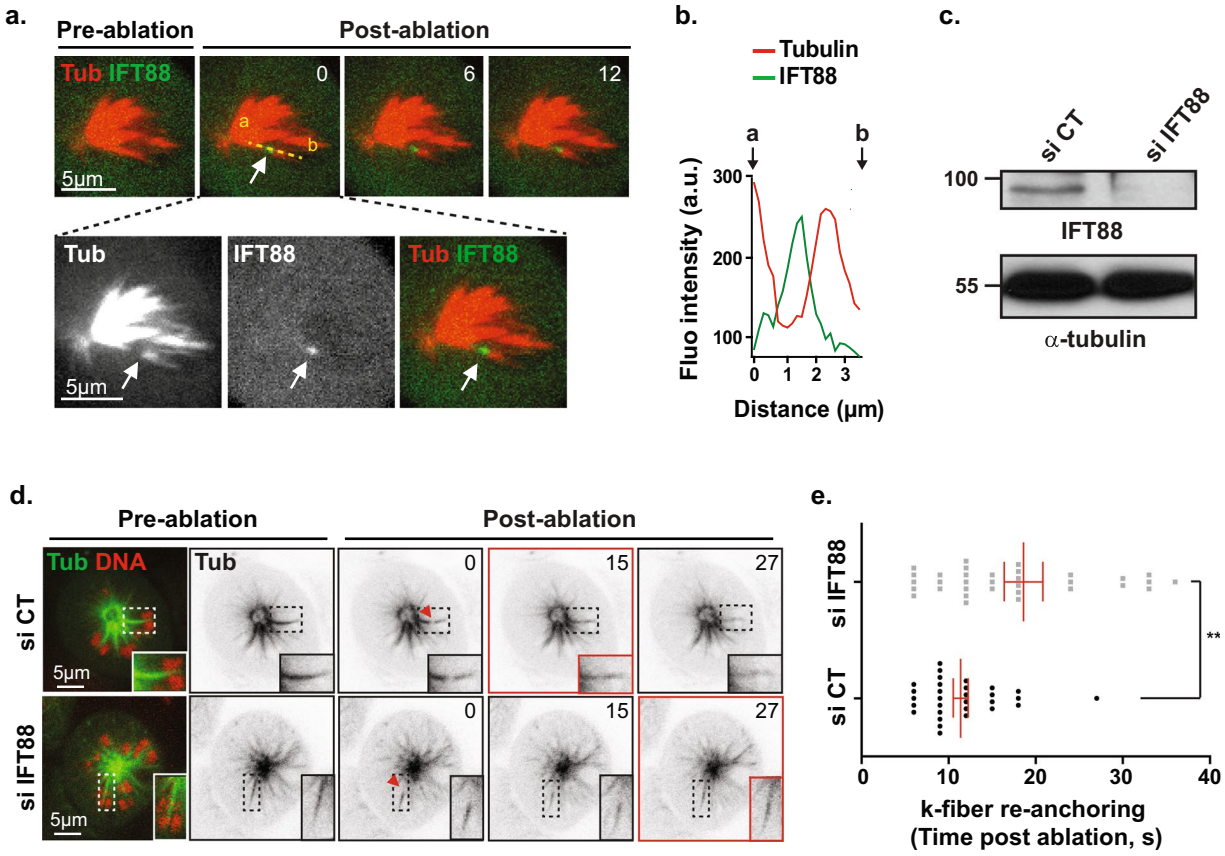


Figure 1. IFT88 is recruited at k-fibers minus-ends after laser ablation and contributes to their re-anchoring into spindle. (**a**) Images from time-lapse microscopy of monopolar Emerald-IFT88 LLC-PK1 cells labelled for tubulin (SiR-Tubulin) before and after k-fiber laser ablation (upper panel). Hoechst live was used to identify k-fibers attached to chromosomes. Time post-ablation (s). α-tubulin, IFT88 and α-tubulin/IFT88 stainings (maximal intensity projection of 2 planes) show IFT88 accumulation at minus-end after laser ablation (white arrow). (**b**) Line scans representing α-tubulin and IFT88 fluorescence intensities measured from a to b along the yellow line shown in (**a**). (**c**) Western-blots showing the amount of IFT88 in GFP-α-tubulin LLC-PK1 cells transfected with control (CT) or IFT88 siRNA. α-tubulin: loading control. (**d**) Images from time-lapse microscopy of monopolar GFP-α-tubulin LLC-PK1 labelled for DNA (Hoechst live, red), to allow for k-fibers detection, in control (CT) and IFT88-depleted cells (left panels). Inverted contrast images of α-tubulin before and after k-fiber ablation (ablation site, red arrowhead) show a delay in k-fiber re-anchoring into spindle upon IFT88 depletion. Images were acquired every 3 s for 2 min. Time post-ablation (s). Single planes are shown. Insets: magnification of the ablated k-fibers, dashed boxes regions. Red boxes indicate k-fibers re-anchoring. (**e**) Quantification of the time (s) required for k-fiber re-anchoring into spindle after laser ablation in CT and IFT88-depleted cells. n ≥ 30 ablated k-fibers (1 ablated k-fiber per cell), 3 experiments. Mean +/− s.e.m $^{**}P < 0.01$ compared to control (*t* test). Scale bars: 5 µm.

NuMA and is required for its enrichment at k-fibers minus-ends after ablation. Taken together, these results show that IFT88 contributes to k-fibers re-anchoring into spindles by allowing NuMA accumulation at the new k-fibers minus-ends generated after ablation.

IFT88 is required for k-fibers re-integration into spindles upon nocodazole washout and for subsequent chromosomes alignment. As an alternative approach to monitor k-fibers reintegration into spindles, we decided to challenge the spindle using nocodazole to depolymerize MTs and monitor spindle reorganization and chromosomes alignment after washout (Fig. 3a–c; Supplementary Movie 4). Indeed, nocodazole washout gives cells the opportunity to nucleate new sets of both centrosomal and acentrosomal MTs, the latest being nucleated in the chromosomal region. These acentrosomal MTs then need to reorganize into k-fibers that rapidly get re-incorporated into the spindle to allow for proper chromosomes alignment. Nocodazole washout therefore gives a unique opportunity to monitor the reorganization and re-incorporation of k-fibers attached to chromosomes into spindles[6,7,21]. In agreement with a role of IFT88 in k-fibers reorganization after nocodazole washout, acentrosomal MTs nucleated in the chromosomal region did not get properly re-incorporated into the main spindle upon IFT88 depletion (Fig. 3a). Indeed, they were delayed in their reincorporation as around 80% of cells still presented with disorganized spindles 5 min after washout compared to 40% in controls (Fig. 3a). Importantly, NuMA minus-end localization was affected by IFT88 depletion as diffuse NuMA staining was

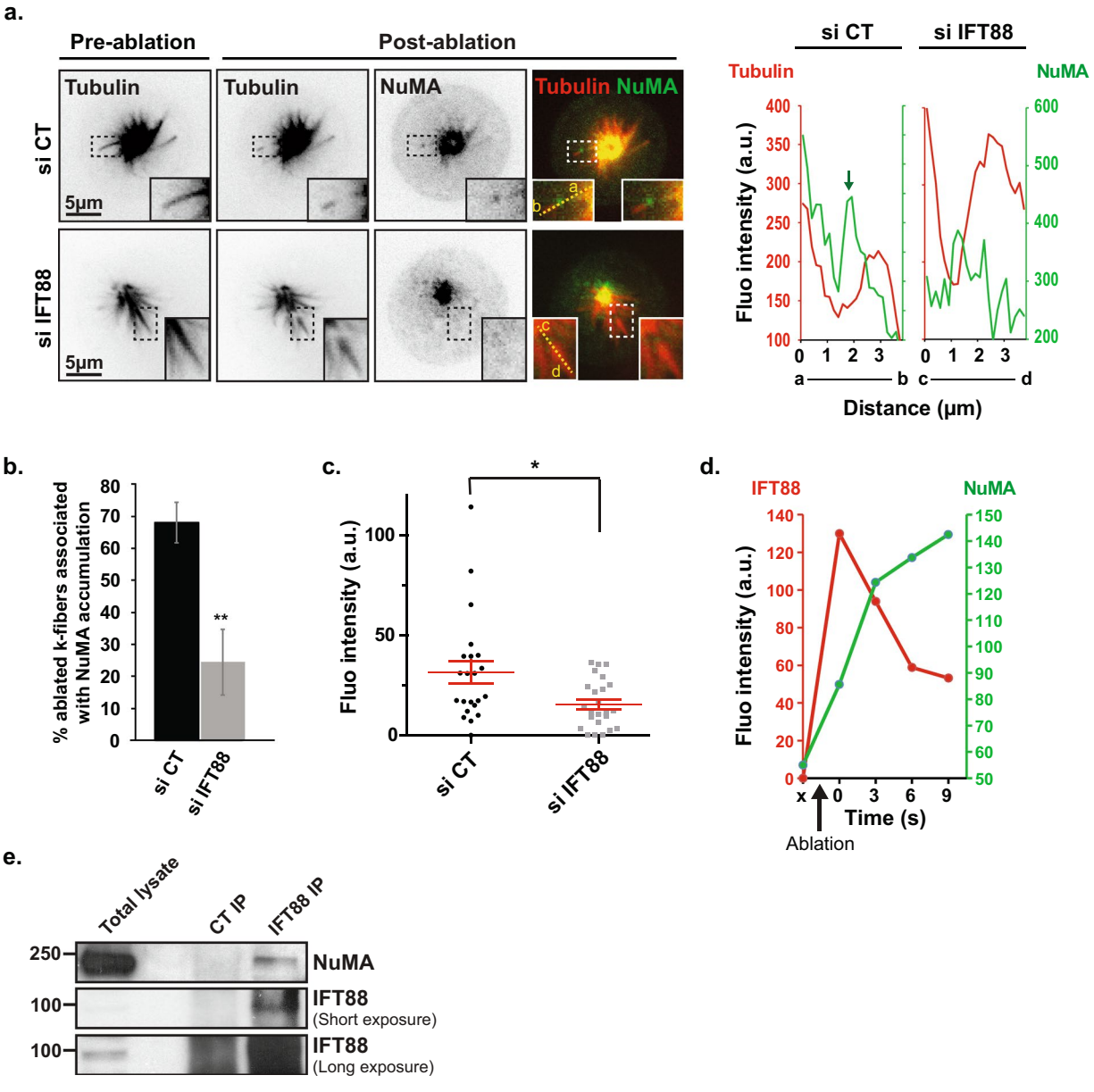


Figure 2. IFT88 interacts with NuMA and contributes to its enrichment at k-fibers minus-ends after laser ablation. (**a**) Inverted contrast and merged images from time-lapse microscopy of monopolar YFP-NuMA LLC-PK1 combined with MT labelling (SiR-Tubulin) in control (CT) and IFT88-depleted cells before and after k-fiber laser ablation. The 3 s time-point after ablation is shown. Single planes are shown. Insets: magnification of the ablated k-fibers, dashed boxes regions. Hoechst live was used to identify k-fibers attached to chromosomes. Line scans (right) representing NuMA and α-tubulin fluorescence intensities, measured from a to b (control) or from c to d (siRNA IFT88) along the yellow line (left inset on the image), show an accumulation of NuMA at minus-ends of k-fibers after laser ablation in CT cells but not in IFT88-depleted cells. Scale bars: 5 µm. (**b**) Percentage of cells with ablated k-fibers associated with NuMA enrichment. $n \geq 29$ ablated k-fibers (1 ablated k-fiber per cell), 3 experiments. Mean +/− s.d. $^{**}P < 0.01$ compared to control (*t* test). (**c**) Quantification of NuMA fluorescence intensity at minus-ends of MT after laser ablation. $n \geq 22$ cells, 2 experiments. Mean +/− s.e.m. $^{*}P < 0.05$ compared to control (*t* test). (**d**) Line scans of IFT88 and NuMA fluorescence intensities overtime at the minus-end of k-fibers after laser ablation. x: pre-ablation; black arrow indicates the time of ablation. (**e**) Endogenous immunoprecipitation of IFT88 performed on LLC-PK1 cells (nocodazole + 3 min washout) shows an interaction with NuMA. Scale bars: 5 µm.

observed compared to intense and focused NuMA signal in the control conditions (Fig. 3b left). Quantifications of NuMA fluorescence intensity at acentrosomal MT asters confirmed this observation (Fig. 3b, right). This result further strengthened the fact that upon nocodazole washout, IFT88 was required for proper NuMA concentration at newly generated acentrosomal MT asters minus-ends and subsequent k-fibers reintegration into spindles.

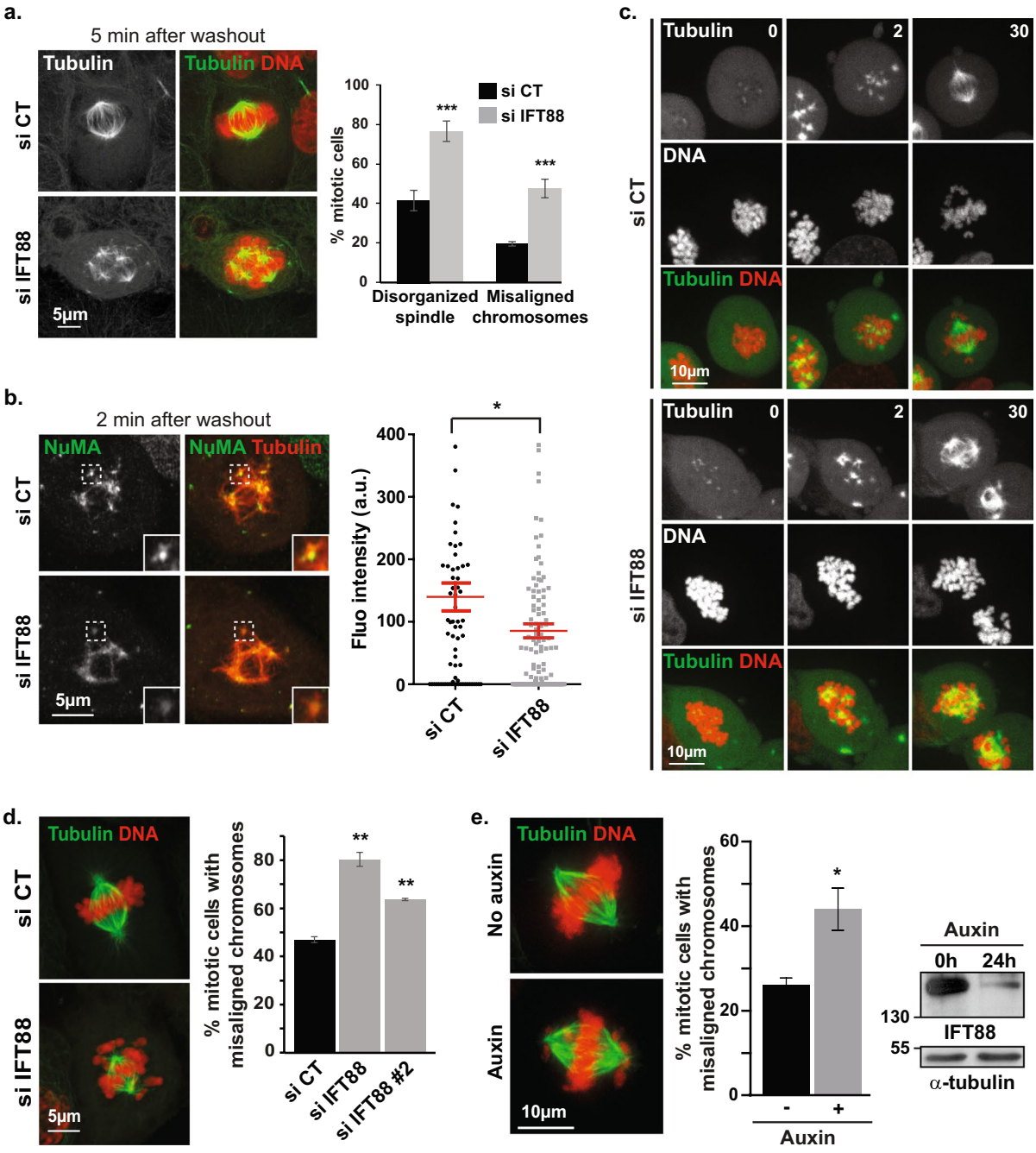


Figure 3. IFT88 contributes to k-fibers reincorporation into spindle after nocodazole washout and is required for proper chromosomes alignment. (**a**) Immunofluorescence images of GFP-α-tubulin LLC-PK1 upon nocodazole treatment followed by 5 min washout showing defects in k-fibers reincorporation into the main spindle in IFT88-depleted cells compared to control. α-tubulin and α-tubulin/DNA stainings are shown (left panel). Percentage of mitotic cells with disorganized spindles or misaligned chromosomes upon nocodazole washout (right panel). n > 300 mitotic cells. 3 experiments. Mean +/− s.d. ***$P < 0.001$ compared to control (*t* test). (**b**) Immunofluorescence images of GFP-α-tubulin LLC-PK1 cells upon nocodazole treatment followed by 2 min washout showing defects in NuMA minus-ends localization in IFT88-depleted cells. NuMA and α-tubulin/NuMA stainings are shown (left panel). Insets: magnified dashed boxes regions. Quantification of NuMA fluorescence intensity at the minus-ends of acentrosomal microtubule asters upon nocodazole washout in control and IFT88-depleted cells (right panel). n ≥ 15 cells per condition and n ≥ 73 acentrosomal microtubule asters per condition, 1 experiment shown, representative of 2 experiments. Mean +/− s.e.m. *$P < 0.05$ compared to control (*t* test). (**c**) Images from time-lapse microscopy of LLC-PK1 GFP-α-tubulin/mCherry-H2B cells showing defects in spindle organization and chromosomes alignment in IFT88-depleted cells compared to control upon nocodazole washout. Time after washout (min). (**d**) Immunofluorescence images of GFP-α-tubulin LLC-PK1 cells showing defects in chromosomes alignment (without nocodazole

challenge) upon IFT88 depletion. α-tubulin/DNA staining is shown (left). Quantification (right): percentage of mitotic cells with misaligned chromosomes (siRNA control, IFT88 and IFT88 #2 as indicated). n > 100 mitotic cells. 3 experiments. Mean +/− s.d. $^{**}P < 0.01$ compared to control (*t* test). (**e**) Immunofluorescence images (left) showing α-tubulin and DNA stainings in HCT116-AID-IFT88 cells. Control (No auxin) and auxin (30 h)-induced AID-YFP-IFT88 degradation conditions are shown. Quantification (middle): percentage of mitotic cells with misaligned chromosomes upon auxin treatment (30 h). n > 50 mitotic cells. 3 experiments. Mean +/− s.e.m $^{*}P < 0.05$ compared to control (*t* test). Western-blots (right) showing AID-YFP-IFT88 depletion in HCT116 cells upon auxin treatment. α-tubulin: loading control. In all panels, maximum projections are shown, scale bars: 5 or 10 μm.

Quantifications also indicated that if most control cells already presented with a visible metaphase plate 5 min after washout with only 19% still showing major chromosomes misalignment, 47% of IFT88-depleted cells still presented with major chromosomes misalignment (Fig. 3a right). Importantly, the delay in spindle reorganization was confirmed by live imaging and correlated with defects in the establishment of a proper metaphase plate (Fig. 3c). Altogether, these observations strengthen the fact that IFT88 is required for the reorganization of k-fibers into spindles, subsequently contributing to proper chromosomes alignment after nocodazole washout. To further validate the requirement of the IFT machinery in chromosomes alignment, we monitored the impact of IFT88 depletion on chromosomes alignment during mitosis without nocodazole challenge. IFT88 depletion, achieved either by siRNA (Fig. 3d) or using a CRISPR-based auxin inducible degron approach (Fig. 3e; Supplementary Fig. 3d), led to defects in chromosomes alignment compared to control condition, thus demonstrating that IFT88 is indeed required for efficient chromosomes alignment in mitosis.

Discussion

Collectively, our results identify a novel role for an IFT protein at k-fibers minus-ends in mitosis. Indeed, taking advantage of MT laser ablation, we show that IFT88 rapidly accumulates at newly generated k-fibers minus-ends upon ablation to efficiently allow their re-anchoring into the main spindle. Moreover, we show here for the first time that IFT88 is required for proper accumulation of NuMA at k-fibers minus-ends in mitosis and that IFT88 can interact with NuMA in mitotic extracts. This finding is strengthened by nocodazole washout experiments that further confirm the requirement of IFT88 for the reorganization of k-fibers into spindles and thus for efficient chromosomes alignment. Taken together, our results are consistent with a model (Fig. 4) in which, upon perturbations of spindle integrity, IFT88 rapidly identifies k-fibers minus-ends (Fig. 4 Step 1) and is required for an efficient minus-ends re-anchoring response by allowing proper NuMA accumulation (Fig. 4 step 2). Such an efficient repair mechanism is important to ensure spindle integrity. Indeed, we propose here that IFT88 would participate in a pathway that provides both flexibility and robustness for the spindle to adapt to perturbations and ensure efficient chromosomes alignment (Fig. 4 steps 1–3).

Our understanding of the mitotic spindle has grown exponentially with the characterization of multiple coexisting MT nucleation pathways that contribute to its assembly, thus ensuring the fidelity of chromosomes segregation[1]. However, we are only starting to understand how all these pathways work together to assemble a functional bipolar spindle and to maintain its integrity. Moreover, all the factors that contribute to the coordination of these different pathways have yet to be fully characterized. NuMA and dynein1 have long been known as factors facilitating spindle assembly and contributing to the maintenance of its integrity[22–26]. Yet, NuMA was only recently shown to provide both spatial and temporal regulation of dynein powered forces[9]. Indeed, MT and k-fibers minus-ends dynamics in mitosis still remain largely less understood than plus-ends dynamics due to the fact that they are embedded into the main spindle and thus difficult to isolate and image. Advanced imaging methods and perturbation tools, including laser ablation, now allow to isolate and track MT minus-ends in space and time[8,27–29]. In this context, our work provides new insights on the regulation of k-fibers dynamics by involving a new player, IFT88, in the control of NuMA local enrichment at minus-ends. By implicating a core member of the IFT machinery in this process, this work strengthens and extends recent works[8,9] since we propose that IFT88 could serve as a mitotic minus-end adaptor to concentrate NuMA at minus-ends subsequently facilitating k-fibers re-incorporation into the spindle.

This work, together with the previously established roles of IFTs in prometaphase[19], provides novel insights on how IFT proteins could control spindle mechanical integrity. We previously showed that, upon mitotic entry, IFTs are required for proper spindle assembly and positioning[19]. Indeed, in association with dynein1, they allow for the assembly of robust astral MT arrays by contributing to peripheral MT clusters re-localization towards the poles. These results, combined to earlier works on dynein1 in transporting peripheral MT and centrosome components, demonstrated that IFTs are required to build the mitotic spindle at the entry of mitosis. We show here that, upon perturbations of spindle mechanics, IFTs are required for spindle repair by allowing a rapid enrichment of proteins, such as NuMA, which is essential for MT and k-fibers minus-ends re-anchoring to mitotic spindle. Indeed, as described previously[9], NuMA accumulation at minus-ends is essential to provide the local activation of dynein leading to MT minus-ends transport towards spindle poles (Fig. 4 step 3). Peripheral MT clusters and k-fibers attached to chromosomes can be considered as 'pre-assembled' parts of the spindle, which are reminiscent of ciliary components for which IFTs serve as cargo inside the cilium[13]. Together, these works place IFTs as cargo adaptors to ensure the spatial accumulation of proteins at both MTs and k-fibers minus-ends and to control spindle mechanical integrity, which in turn is essential to ensure proper chromosomes alignment. Whether IFTs only contribute to chromosomes alignment by controlling spindle integrity or whether they could also act elsewhere, for example at the kinetochore, will require further investigations. Of note, IFTs also serve as cargo adaptors at later mitotic stages to control central spindle organization[20].

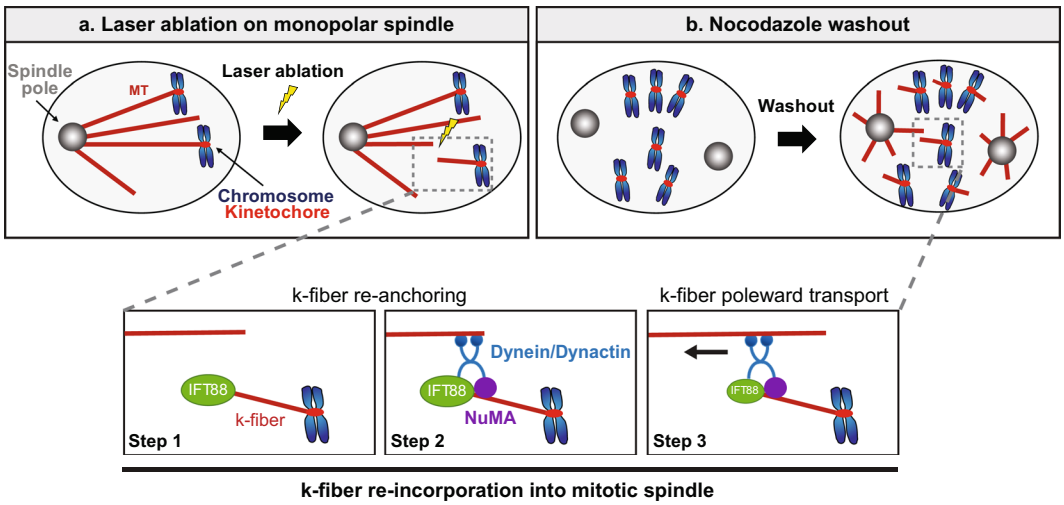


Figure 4. Model for IFT88 function in k-fibers re-anchoring into mitotic spindles. Upon perturbations, including MT laser ablation (**a**) or nocodazole washout (**b**), IFT88 rapidly accumulates (step 1) at newly generated minus-ends and is required for an efficient minus-ends re-anchoring response of k-fibers by allowing proper NuMA accumulation (step 2). As described previously, NuMA would then be required to target dynein activity to minus-ends through dynactin recruitment subsequently allowing poleward transport of k-fibers (step 3). In this model, IFT88 would serve as a mitotic minus-end adaptor to concentrate NuMA at minus-ends thus facilitating k-fibers re-anchoring into the main spindle.

The mitotic spindle is a highly dynamic structure that requires a robust molecular machinery to maintain its integrity[1,2,30]. If the major pathways for spindle assembly have been extensively characterized, a lot still has to be uncovered on less studied spindle assembly factors that contribute to its integrity, including IFT proteins. This is particularly important for spindle assembly pathways involved in error detection and correction. Indeed, these alternative pathways are crucial to ensure proper chromosomes alignment and segregation and proper completion of mitosis. Future works, including *in vitro* studies to avoid the complexity of the cellular context, will address which IFT proteins participate in the maintenance of spindle mechanical integrity, how IFT sub-complexes interact with MT minus-ends and how their recruitment is regulated. Such experiments will indeed be key to unravel how IFTs, MAPs and motor proteins sequentially get recruited to MT minus-ends and will allow to fully understand contribution of the IFT machinery to spindle mechanical integrity. By characterizing a novel cilia-independent function for an IFT at the minus-ends of k-fibers, this work complements recent evidences that introduce new perspectives on cellular processes involving IFT proteins beyond their role in cilia. These include, in addition to cell cycle[31] and cell division[19,20,32], immune synapse polarization[17,18,33], cell migration[34] and the regulation of cytoplasmic MT dynamics[16,35] or actin[36]. Future works will be required to address whether IFTs function in these non-ciliary roles only as cargo adaptors or also as motor regulators as shown for ciliary motors[15].

Methods

Cell culture. LLC-PK1 (CLS Cell Lines Services GmbH, Germany), GFP-αtubulin LLC-PK1 (Gift from P. Wadsworth)[5], GFP-αtubulin/mCherry-H2B LLC-PK1 previously generated[20] and YFP-NuMA LLC-PK1 cells were grown in a 1:1 mixture of Opti-MEM/HAM's F10 media supplemented with 10% fetal bovine serum (FBS). HCT116-IFT88-AID, previously generated[20], were grown in DMEM Glutamax medium supplemented with 10% FBS. YFP-NuMA and mEmerald-IFT88 LLC-PK1 cells were generated by transfection of LLC-PK1 with pEYFP-C1-NuMA (Addgene plasmid #28238) or mEmerald-IFT88-N-18 (Addgene plasmid #54125). Cells were then selected with G418 and sorted based on their fluorescence. SiR Tubulin and Hoechst live were added before starting live experiments for 2 h at 100 nM and for 30 min at 5 µg/ml respectively.

Cell synchronization, inhibitors and microtubules regrowth assays. For immunoprecipitation experiments, LLC-PK1 cells were synchronized in mitosis using nocodazole 100 ng/ml (Sigma-Aldrich) for 15 h. Cells were then incubated for 5 min on ice and nocodazole was removed by washing twice in cold PBS. Cells were then released in cold medium and placed at 37 °C for MTs to regrow before collecting cells and proceeding with lysis. To induce monopolar spindles, LLC-PK1 cells were treated with the kinesin-5 inhibitor S-trityl-l-cysteine (STLC, Santa Cruz) 2 µM for 15 h. For MT regrowth assays, cells transfected for 48 h with siRNA were treated with 100 ng/ml nocodazole (Sigma-Aldrich) in culture medium ON at 37 °C to depolymerize MTs. Cells were placed on ice for 10 min and washed three times with 4 °C PBS. Cells were then incubated in 37 °C culture medium without nocodazole and kept at 37 °C to allow regrowth. Cells were fixed in MeOH at the indicated time after washout and processed for immunofluorescence. For live imaging, after nocodazole washout in 4 °C PBS, cells were incubated in 4 °C culture medium instead of 37 °C to delay regrowth in order to facilitate imaging and then placed in the 37 °C chamber for imaging.

AID cell line, siRNA and cDNA transfections. Targeted proteins were depleted with small-interfering RNAs (siRNAs) designed and ordered via Dharmacon (Lafayette, CO; siRNA IFT88 5′-CCUUGGAGAUCGAGAGAAUU-3′; siRNA IFT88 #2 5′-CCGAGGAGUUGGAGAAUGAUU-3′) and delivered to cells at a final concentration of 100 nM using Oligofectamine (Invitrogen, Carlsbad, CA) according to manufacturers' instructions. The efficacy of proteins knockdown was assessed by immunoblotting 48 h post transfection. HCT116-IFT88-AID cells were generated as previously described[20]. Targeting of IFT88 and degradation of IFT88-AID-YFP was confirmed by western-blot following addition of Auxin (Sigma-Aldrich) at 500 μM in the culture medium for 24 h. cDNA transfections were performed using JetPEI (Polyplus Transfection) or Fugene 6 (Promega) transfection reagents according to manufacturers' instructions for 24 h. cDNAs transfected include pEYFP-C1-NuMA (gift from Michael Mancini; Addgene plasmid # 28238; http://n2t.net/addgene:28238; RRID: Addgene_28238) and mEmerald-IFT88-N-18 (gift from Michael Davidson; Addgene plasmid # 54125; http://n2t.net/addgene:54125; RRID: Addgene_54125).

Lysates, immunoprecipitations and immunoblotting. LLC-PK1 and HCT116 cell extracts were obtained after lysis with buffer containing 50 mM Hepes (pH 7.5), 150 mM NaCl, 1.5 mM $MgCl_2$, 1 mM EGTA, 1% IGEPAL CA-630 and protease inhibitors (Sigma-Aldrich). Protein concentration for lysates was determined using Bradford reagent (Sigma-Aldrich), loads were adjusted and proteins were resolved by SDS-PAGE and analyzed by western-blot (Western Lightning Plus-ECL kit; PerkinElmer). For endogenous immunoprecipitations, LLC-PK1 cells were synchronized in mitosis using nocodazole and washout was done for 3 min at 37 °C. The resulting cell extracts were incubated for 2 h at 4 °C with IFT88 antibody or rabbit IgG (3 mg of total extracts and 2 μg of antibody) and then incubated for 45 min with protein G-PLUS agarose beads (Santa Cruz; sc-2002). Beads were washed three times with 500 μl lysis buffer and the immunoprecipitated proteins were separated by SDS-PAGE and analyzed by western blotting.

Antibodies. The following primary antibodies were used (western-blot WB, immunofluorescence IF, immunoprecipitation IP): IFT88 #13967-1-AP (WB: 1/500, IF: 1/250, IP: 2 μg) from Proteintech, α-tubulin (DM1α, Sigma-Aldrich #T6199, WB: 1/400), FITC-conjugated α-tubulin (DM1α, Sigma-Aldrich #F2168, IF: 1/300), NuMA (Santa-Cruz sc-365532 IF: 1:200; Abcam ab-36999 WB: 1/500) and DAPI (Cell signaling, IF: 1/10000). IgG from rabbit serum (Sigma-Aldrich I5006) were used as control IP. Secondary antibodies include for IF: Alexa Fluor 488 (#4412S or #4408S) or 555 (#4413 S or #4409S) -conjugated anti-rabbit or anti-mouse secondary antibodies (Molecular Probes, 1/1500) and for WB: anti-mouse and anti-rabbit IgG, HRP linked antibody (Cell signaling #7076 and #7074, 1/5000).

Immunofluorescence. For immunofluorescence experiments, cells were fixed in −20 °C MeOH to preserve MTs staining. Then, cells were blocked with PBS-BSA 1%-Triton 0.5% and stained for immunofluorescence with the appropriate primary and secondary antibodies. Slides were mounted in prolong gold (Life Technologies).

Microscopy, laser ablation and image analysis. Epifluorescence images of the auxin inducible degron experiment were acquired with a Leica DM6000 microscope (Objective: 63x/1.4 NA Plan-Apo) equipped with a Cool SNAP HQ2 camera and controlled by MetaMorph (Molecular Devices). Confocal images and time-lapse were performed using a spinning disk confocal microscope, a Nikon Ti Eclipse coupled to a Yokogawa spinning disk head and an EMCCD iXon Ultra camera (60x/1.4 NA), controlled by the Andor iQ3 software (Andor) or a Zeiss confocal LSM880 (Objective 63x/1.4 NA) controlled by Zen (Zeiss). For laser ablation experiments, the spinning disk confocal microscope (Objective 60x/1.4 NA; optovar 1.5) is coupled to the MicroPoint system (Andor) equipped with a pulsed nitrogen pumped tunable dye laser capable of MT ablation (wavelength 551 nm, frequency 10 Hz, repetition rate 10, number of repeats 5). Three images (plane of the ablation) were acquired at 1 s interval before the ablation, then images were acquired every 3 s for 2 min (5 planes over 4 μm; centered on the plane of the ablation). Of note, there is about 1 s between the end of the ablation (micropoint ablation module, Andor) and the first acquisition. For nocodazole washout experiments, images were acquired every 15 s (maximum projections are shown, 11 planes over 10 μm). Image processing and analysis were performed with ImageJ: cropping, rotating, brightness, contrast adjustment, color combining and fluorescence intensity measurements (fluorescence intensity of the region of interest minus fluorescence intensity of a background region of the same size inside the cell; sum projection of all planes). Line scans were obtained using ImageJ plot profile tool. Movies were generated with MetaMorph (Molecular Devices) and displayed at 3 or 10 frames per second as indicated.

Statistical analysis. The number of cells counted per experiment for statistical analysis is indicated in figure legends. Graphs were created using Microsoft Excel or GraphPad Prism software and error bars represent the s.d. or s.e.m. as indicated. p-values were calculated using a two-tailed Student's t test. $p > 0.05$ was considered as not significant and by convention $*p < 0.05$, $**p < 0.01$ and $***p < 0.001$.

Data Availability

The authors declare that the main data supporting the findings of this study are available within the article.

References

1. Prosser, S. L. & Pelletier, L. Mitotic spindle assembly in animal cells: a fine balancing act. *Nat. Rev. Mol. Cell Biol.* **18**, 187–201 (2017).
2. Meunier, S. & Vernos, I. Acentrosomal Microtubule Assembly in Mitosis: The Where, When, and How. *Trends Cell Biol.* **26**, 80–87 (2016).
3. Meunier, S. & Vernos, I. Microtubule assembly during mitosis - from distinct origins to distinct functions? *J. Cell Sci.* **125**, 2805–2814 (2012).
4. Tulu, U. S., Rusan, N. M. & Wadsworth, P. Peripheral, non-centrosome-associated microtubules contribute to spindle formation in centrosome-containing cells. *Curr. Biol. CB* **13**, 1894–1899 (2003).

5. Rusan, N. M., Tulu, U. S., Fagerstrom, C. & Wadsworth, P. Reorganization of the microtubule array in prophase/prometaphase requires cytoplasmic dynein-dependent microtubule transport. *J. Cell Biol.* **158**, 997–1003 (2002).
6. Khodjakov, A., Copenagle, L., Gordon, M. B., Compton, D. A. & Kapoor, T. M. Minus-end capture of preformed kinetochore fibers contributes to spindle morphogenesis. *J. Cell Biol.* **160**, 671–683 (2003).
7. Maiato, H., Rieder, C. L. & Khodjakov, A. Kinetochore-driven formation of kinetochore fibers contributes to spindle assembly during animal mitosis. *J. Cell Biol.* **167**, 831–840 (2004).
8. Elting, M. W., Hueschen, C. L., Udy, D. B. & Dumont, S. Force on spindle microtubule minus ends moves chromosomes. *J. Cell Biol.* **206**, 245–256 (2014).
9. Hueschen, C. L., Kenny, S. J., Xu, K. & Dumont, S. NuMA recruits dynein activity to microtubule minus-ends at mitosis. *eLife* **6** (2017).
10. Akhmanova, A. & Steinmetz, M. O. Control of microtubule organization and dynamics: two ends in the limelight. *Nat. Rev. Mol. Cell Biol.* **16**, 711–726 (2015).
11. Rosenbaum, J. L. & Witman, G. B. Intraflagellar transport. *Nat. Rev. Mol. Cell Biol.* **3**, 813–825 (2002).
12. Stepanek, L. & Pigino, G. Microtubule doublets are double-track railways for intraflagellar transport trains. *Science* **352**, 721–724 (2016).
13. Bhogaraju, S. *et al*. Molecular basis of tubulin transport within the cilium by IFT74 and IFT81. *Science* **341**, 1009–1012 (2013).
14. Lechtreck, K. F., Van De Weghe, J. C., Harris, J. A. & Liu, P. Protein transport in growing and steady-state cilia. *Traffic Cph. Den.* **18**, 277–286 (2017).
15. Mohamed, M. A. A., Stepp, W. L. & Ökten, Z. Reconstitution reveals motor activation for intraflagellar transport. *Nature* **557**, 387–391 (2018).
16. Bizet, A. A. *et al*. Mutations in TRAF3IP1/IFT54 reveal a new role for IFT proteins in microtubule stabilization. *Nat. Commun.* **6**, 8666 (2015).
17. Finetti, F. *et al*. Specific recycling receptors are targeted to the immune synapse by the intraflagellar transport system. *J. Cell Sci.* **127**, 1924–1937 (2014).
18. Finetti, F. *et al*. Intraflagellar transport is required for polarized recycling of the TCR/CD3 complex to the immune synapse. *Nat. Cell Biol.* **11**, 1332–1339 (2009).
19. Delaval, B., Bright, A., Lawson, N. D. & Doxsey, S. The cilia protein IFT88 is required for spindle orientation in mitosis. *Nat. Cell Biol.* **13**, 461–468 (2011).
20. Taulet, N. *et al*. IFT proteins spatially control the geometry of cleavage furrow ingression and lumen positioning. *Nat. Commun.* **8**, 1928 (2017).
21. Tulu, U. S., Fagerstrom, C., Ferenz, N. P. & Wadsworth, P. Molecular requirements for kinetochore-associated microtubule formation in mammalian cells. *Curr. Biol. CB* **16**, 536–541 (2006).
22. Merdes, A., Heald, R., Samejima, K., Earnshaw, W. C. & Cleveland, D. W. Formation of spindle poles by dynein/dynactin-dependent transport of NuMA. *J. Cell Biol.* **149**, 851–862 (2000).
23. Merdes, A., Ramyar, K., Vechio, J. D. & Cleveland, D. W. A complex of NuMA and cytoplasmic dynein is essential for mitotic spindle assembly. *Cell* **87**, 447–458 (1996).
24. Heald, R. *et al*. Self-organization of microtubules into bipolar spindles around artificial chromosomes in Xenopus egg extracts. *Nature* **382**, 420–425 (1996).
25. Verde, F., Berrez, J. M., Antony, C. & Karsenti, E. Taxol-induced microtubule asters in mitotic extracts of Xenopus eggs: requirement for phosphorylated factors and cytoplasmic dynein. *J. Cell Biol.* **112**, 1177–1187 (1991).
26. Gaglio, T., Saredi, A. & Compton, D. A. NuMA is required for the organization of microtubules into aster-like mitotic arrays. *J. Cell Biol.* **131**, 693–708 (1995).
27. Lecland, N. & Lüders, J. Imaging and Quantifying the Dynamics of γ-Tubulin at Microtubule Minus Ends in Mitotic Spindles. *Methods Mol. Biol. Clifton NJ* **1413**, 63–75 (2016).
28. Sikirzhytski, V. *et al*. Direct kinetochore-spindle pole connections are not required for chromosome segregation. *J. Cell Biol.* **206**, 231–243 (2014).
29. Milas, A., Jagrić, M., Martinčić, J. & Tolić, I. M. Optogenetic reversible knocksideways, laser ablation, and photoactivation on the mitotic spindle in human cells. *Methods Cell Biol.* **145**, 191–215 (2018).
30. Sánchez-Huertas, C. & Lüders, J. The augmin connection in the geometry of microtubule networks. *Curr. Biol. CB* **25**, R294–299 (2015).
31. Robert, A. *et al*. The intraflagellar transport component IFT88/polaris is a centrosomal protein regulating G1-S transition in non-ciliated cells. *J. Cell Sci.* **120**, 628–637 (2007).
32. Borovina, A. & Ciruna, B. IFT88 plays a cilia- and PCP-independent role in controlling oriented cell divisions during vertebrate embryonic development. *Cell Rep.* **5**, 37–43 (2013).
33. Galgano, D. *et al*. The T cell IFT20 interactome reveals new players in immune synapse assembly. *J. Cell Sci.* **130**, 1110–1121 (2017).
34. Boehlke, C. *et al*. A Cilia Independent Role of Ift88/Polaris during Cell Migration. *PloS One* **10**, e0140378 (2015).
35. Dupont, M. A. *et al*. Human IFT52 mutations uncover a novel role for the protein in microtubule dynamics and centrosome cohesion. *Hum. Mol. Genet*, https://doi.org/10.1093/hmg/ddz091 (2019).
36. Wang, Z. *et al*. IFT88 influences chondrocyte actin organization and biomechanics. *Osteoarthritis Cartilage* **24**, 544–554 (2016).

Acknowledgements

The experiments were performed within the France-BioImaging national research (ANR-10-INSB-04, "Investments for the future"), at Montpellier Ressources Imagerie facility (MRI), Montpellier. We thank the engineers on the MRI facility, Simon Descamps and Audrey Guesdon for their help with cell culture and buffers and the members of the team for discussions on the project. This work was supported by the ANR "Chaire d'excellence" CilMitoCyst (ANR-12-CHEX-005 to B.D.), the Marie Curie career integration grant (CilMitoPatho to BD), the Fondation pour la Recherche Médicale (Partenariat Fondation Schlumberger pour l'Education et la Recherche to B.D.), the Fondation ARC pour la Recherche sur le Cancer (B.D.) and the CNRS (B.V., C.A., B.D.).

Author Contributions

B.D. and N.T. jointly conceived and supervised the project, designed and analyzed the experimental work, assembled the figures and wrote the manuscript. N.T. technically trained A.D. and they executed the experimental work. N.T. drew the model presented in Fig. 4. C.A. helped with cell culture. B.V. carried out and analyzed the Auxin inducible degron data with the technical help of J.M. and helped with manuscript editing. V.G. and Y.D. set up the MicroPoint module on the MRI platform and together with N.T. optimized it for M.T. laser ablation.

Additional Information

Supplementary information accompanies this paper at https://doi.org/10.1038/s41598-019-46605-x.

Competing Interests: The authors declare no competing interests.

Publisher's note: Springer Nature remains neutral with regard to jurisdictional claims in published maps and institutional affiliations.

Open Access This article is licensed under a Creative Commons Attribution 4.0 International License, which permits use, sharing, adaptation, distribution and reproduction in any medium or format, as long as you give appropriate credit to the original author(s) and the source, provide a link to the Creative Commons license, and indicate if changes were made. The images or other third party material in this article are included in the article's Creative Commons license, unless indicated otherwise in a credit line to the material. If material is not included in the article's Creative Commons license and your intended use is not permitted by statutory regulation or exceeds the permitted use, you will need to obtain permission directly from the copyright holder. To view a copy of this license, visit http://creativecommons.org/licenses/by/4.0/.

© The Author(s) 2019